NIH Public Access
Author Manuscript
Bioorg Med Chem. Author manuscript; available in PMC 2011 December 15.

Published in final edited form as:
Bioorg Med Chem. 2010 December 15; 18(24): 8592–8599. doi:10.1016/j.bmc.2010.10.018.

A Novel PET Marker for *In Vivo* Quantification of Myelination

Chunying Wu[a], **Changing Wang**[a], **Daniela Popescu**[b], **Wenxia Zhu**[a], **Eduardo Somoza**[a], **Junqing Zhu**[a], **Allison G. Condie**[a], **Chris Flask**[a], **Robert H. Miller**[b], **Wendy Macklin**[c], and **Yanming Wang**[a,*]

[a] Division of Radiopharmaceutical Science, Case Center for Imaging Research, Department of Radiology, Case Western Reserve University, Cleveland, OH 44106

[b] Department of Neurosciences, Case Western Reserve University, Cleveland, OH 44106

[c] Department of Cell and Developmental Biology, University of Colorado Denver Health Sciences, Aurora, CO 80045

Abstract

C-11-Labeled *N*-methyl-4,4′-diaminostilbene ([^{11}C]MeDAS) was synthesized and evaluated as a novel radiotracer for *in vivo* microPET imaging of myelination. [^{11}C]MeDAS exhibits optimal lipophilicity for brain uptake with a logPoct value of 2.25. Both *in vitro and ex vivo* staining exhibited MeDAS accumulation in myelinated regions such as corpus callosum and striatum. The corpus callosum region visualized by MeDAS is much larger in the hypermyelinated *Plp*-Akt-DD mouse brain than in the wild-type mouse brain, a pattern that was also consistently observed in Black-Gold or MBP antibody staining. *Ex vivo* autoradiography demonstrated that [^{11}C]MeDAS readily entered the mouse brain and selectively labeled myelinated regions with high specificity. Biodistribution studies showed abundant initial brain uptake of [^{11}C]MeDAS with 2.56% injected dose/whole brain at 5 min post injection and prolonged retention in the brain with 1.37% injected dose/whole brain at 60 min post injection. An *in vivo* pharmacokinetic profile of [^{11}C]MeDAS was quantitatively analyzed through a microPET study in an *Plp*-Akt-DD hypermyelinated mouse model. MicroPET studies showed that [^{11}C]MeDAS exhibited a pharmacokinetic profile that readily correlates the radioactivity concentration to the level of myelination in the brain. These studies suggest that MeDAS is a sensitive myelin probe that provides a direct means to detect myelin changes in the brain. Thus, it can be used as a myelin-imaging marker to monitor myelin pathology *in vivo*.

Keywords

myelin; imaging; positron emission tomography (PET); magnetic resonance imaging (MRI); hypermyelination

© 2010 Elsevier Ltd. All rights reserved.

Correspondence should be addressed to: Yanming Wang, PhD Division of Radiopharmaceutical Science, Case Center for Imaging Research, Department of Radiology, Case Western Reserve University, Cleveland, OH 44106. Tel. 216 844 3288. Fax. 216 844 8062. yanming.wang@case.edu.

Publisher's Disclaimer: This is a PDF file of an unedited manuscript that has been accepted for publication. As a service to our customers we are providing this early version of the manuscript. The manuscript will undergo copyediting, typesetting, and review of the resulting proof before it is published in its final citable form. Please note that during the production process errors may be discovered which could affect the content, and all legal disclaimers that apply to the journal pertain.

NIH-PA Author Manuscript
NIH-PA Author Manuscript
NIH-PA Author Manuscript

NIH-PA Author Manuscript

NIH-PA Author Manuscript

NIH-PA Author Manuscript

1. INTRODUCTION

In the central nervous system (CNS), myelin membranes play a critical role in protecting neurons for speedy and accurate signal transduction.[1] Destruction of or changes in myelination are considered some of the primary causes of neurological disorders such as multiple sclerosis (MS).2,3 Current efforts have focused on the delineation of molecular mechanisms of myelination and the development of novel therapies aimed at the prevention of demyelination and the promotion of remyelination.4 These studies require a molecular imaging tool that permits direct detection and quantification of myelin changes *in vivo*.

Thus far, magnetic resonance imaging (MRI) has been the primary modality in brain imaging to detect lesions associated with the destruction and/or repair of myelin.5-8 Because any change in MRI signal intensity reflects only a change in tissue water content, many other macroscopic tissue injuries that affect water content, such as inflammation and edema, can also be visualized by MRI. As a result, MRI signal intensities are not specific for myelin changes. Indeed, use of MRI has been found to be dissociated from clinical outcomes of current therapies for MS.9 It is thus necessary to develop a direct imaging marker that is specific for changes in myelin content. For this reason, we set out to develop myelin-imaging agents for positron emission tomography (PET). PET is a functional imaging technique that is suitable for *in vivo* studies of biochemical and metabolic processes at the molecular level.[10] For directly monitoring myelin changes in the brain, appropriate radiotracers must be developed that readily penetrate the blood-brain barrier (BBB) and localize in brain regions in proportion to the extent of myelination. Once developed, these radiotracers can be used in conjunction with PET as a novel imaging marker to directly and quantitatively assess the extent of demyelination or remyelination. This will provide a direct clinical efficacy endpoint measure of myelin change and become a potentially powerful tool in efficacious evaluation of myelin repair therapies.

Currently, a very limited number of small-molecule probes (SMP) for PET imaging of myelination *in vivo* studies have been developed in MS as represented by [^{11}C]PK11195, which is a radiotracer developed to characterize peripheral benzodiazepine receptors (PBR) expressed by microglial cells.[11] [^{11}C]PK11195-PET is often used to study the correlation of microglia activation with tissue destruction and disease progression in MS patients.[12,13] However, [^{11}C]PK11195-PET is not a specific marker of demyelination, a hallmark that is characteristic of MS. [^{11}C]PK11195-PET imaging is capable of imaging only inflammation and does not provide any correlation of disease progression with the degree of myelination in the brain.

Recently, we have studied a novel series of stilbene derivatives as myelin imaging agents, which show promising binding properties with high affinity and specificity for myelin.[14] Based on structure-activity relationship studies, we have identified a lead agent, termed MeDAS, that is suitable for *in vivo* imaging studies. In continuation of our previous work,[14] we radiolabeled MeDAS with C-11 and conducted a series of *in vitro*, *ex vivo*, and *in vivo* studies including tissue staining, biodistribution, autoradiography, and microPET in a transgenic *Plp*-Akt-DD mouse model. In this model, myelination in the brain is enhanced as a result of over expression of serine/threonine kinase Akt, leading to hypermyelination in the white matter regions, especially in the corpus callosum.[15] These studies are designed to validate [^{11}C]MeDAS as a promising SMP for PET imaging of myelination *in vivo*. Compared to immuno-PET, which requires use of radiolabeled antibodies, SMP-PET is advantageous in that radiosynthesis of the imaging agents is more practical and their structures and pharmacokinetics can be clearly characterized. *In vivo* [^{11}C]MeDAS-PET studies in *Plp*-Akt-DD mice in comparison with normal controls showed that [^{11}C]MeDAS is a sensitive and specific radiotracer for PET imaging of myelination.

NIH-PA Author Manuscript

NIH-PA Author Manuscript

NIH-PA Author Manuscript

2. Results and Discussion

2.1 Radiochemistry

The synthesis of the target [^{11}C]MeDAS was accomplished using (*E*)-4,4′-diaminostilbene (DAS) in acetone with [^{11}C]methyl triflate ([^{11}C]CH_3OTf) as outlined in Scheme 1. The cyclotron-derived [^{11}C]carbon dioxide was converted to [^{11}C]methyl iodide ([^{11}C]CH_3I) by an automatic synthesis modular FXc-box (General Electric Medical Systems) using the direct iodination of [^{11}C]methane produced by an on-site cyclotron. [^{11}C]CH_3OTf was generated by reaction of the produced [^{11}C]CH_3I with silver triflate (fixed on a column) at 200°C. The [^{11}C]CH_3OTf was then bubbling into a reaction vial prefilled with 1-2 mg of DAS dissolved in 0.5 mL acetone at −30 °C. The radiomethylation reaction was then carried out at 90°C for 2 min. After cooling to room temperature the reaction mixture was diluted with 1 mL of HPLC eluent and was subsequently transferred to a semi-preparative radio-HPLC system. (Phenomenex C-18 column, 10 μ, 250 mm × 10 mm, acetonitrile : H_2O = 60 : 40, flow rate 8.0 mL/min). Under these conditions, the retention time of the precursor DAS was 2.95 min. The fraction containing the product (retention time: 5.01 min) was collected and diluted with sterile water. The resulting mixture was subjected to solid-phase extraction using a C-18 Sep-Pak cartridge. The Sep-Pak was washed with another 10 mL of water and the final product was eluted with 1 mL of ethanol followed by 9 mL of sterile saline to formulate the product as isotonic solution. The synthesis was completed in 50 - 60 min. The decay-corrected radiochemical yield of [^{11}C]MeDAS obtained was in the range of 50 - 60%.

Quality control of the product was carried out by an analytical radio-HPLC system (Phenomenex C-18 column, 5 μ, 250 mm × 4.6 mm, acetonitrile : H_2O = 60 : 40, flow rate 1.0 mL/min). As shown in Figure 1A, the retention time of the precursor (DAS) and non-labeled product (MeDAS) were 4.57 min and 6.77 min, respectively. The quantity of the precursor DAS in the final product is negligible. As shown in Figure 1B, no DAS residue was detected by HPLC after purification. Identification of the product was verified by co-injection with the non-labeled standard of MeDAS. As shown in Figure 1C, the retention time of [^{11}C]MeDAS was 6.77 min, which is consistent with the cold standard. Quality control by radio-HPLC showed a radiochemical purity of > 95%. The specific activity of [^{11}C]MeDAS was determined as 80 ± 30 GBq/μmol (end of synthesis, EOS).

2.2 Lipophilicity

Under physiological pH, [^{11}C]MeDAS exists as a neutral molecule. Following radiolabelling, the lipophilicity of [^{11}C]MeDAS was determined in terms of its partition coefficient between water and *n*-octanol (logPoct). Lipophilicity is an important factor in brain permeability. Previous studied have shown that small-molecule compounds with a logPoct value ranging from 1.5-3.5 normally exhibit optimal brain uptake.[16,17] Using the conventional octanol-water partition method, we determined the logPoct value of [^{11}C]MeDAS as 2.25 ± 0.23 (n=3). This value falls into the range for optimal brain permeability.

2.3 Brain uptake and whole body biodistribution studies

After radiosynthesis, brain uptake and the biodistribution of [^{11}C]MeDAS were evaluated in normal mice. Generally, the biodistribution study provides critical information on brain permeability and other pharmacokinetic properties. As shown in Table 1, a significant uptake was observed in the brain. [^{11}C]MeDAS displayed a high brain uptake at an early time point with 2.56% ID/organ at 5 min, which was about 5-6 fold higher than that of [^{11}C]PK11195 at the corresponding time point,[18] as well as a prolonged retention at a later time point with 1.37% ID/organ at 60 min. [^{11}C]MeDAS can thus freely pass across the

NIH-PA Author Manuscript

NIH-PA Author Manuscript

NIH-PA Author Manuscript

blood-brain barrier. The initial brain uptake of 2-3%ID at 2-5 min after iv injection is sufficient for imaging studies. Whole body biodistribution studies also showed that liver and kidney are the major organs that exhibited relatively high uptake of [^{11}C]MeDAS at early time point (15.86%ID/organ and 2.69 %ID/organ at 5 min, respectively).

2.4 Histochemistry

2.4.1 *In vitro* staining of myelin sheaths in *Plp*-Akt-DD and wild type mice— MeDAS exhibits a remarkably high myelin-binding affinity based on spectrophotometry and radioligand binding assays.[14] *In vitro* tissue staining of mouse brain tissue sections showed that the MeDAS selectively stained myelinated regions. We then examined if MeDAS could differentiate the quantity of myelin present in hypermyelinated *Plp*-Akt-DD mice and control littermates *in vitro*. *Plp*-Akt-DD is a transgenic mouse model in which myelination in the brain is enhanced due to the over-expression of serine/threonine kinase Akt. In parallel to MeDAS staining, immunohistochemical staining for myelin-specific MBP and Black-Gold staining were also conducted on adjacent sections for comparison. MeDAS is a fluorescent compound that can be used directly for tissue staining. At 10 μM concentration, MeDAS selectively labeled myelinated regions such as the corpus callosum (Figure 2A, 2D). To confirm that staining was truly associated with binding to myelin sheaths, we compared MeDAS staining with other conventional immunohistochemical staining of the adjacent sections from each mouse brain. As shown in Figure 2, the pattern of MeDAS staining in *Plp*-Akt-DD mice and control littermates were identical with that of Black-Gold staining (Figure 2B, 2E) and MBP staining (Figure 2C, 2F) in adjacent sections. In addition, MeDAS staining is found to be as sensitive as antibody staining. These results suggest that MeDAS staining of the corpus callosum and striatum is dependent on the presence of myelin. The corpus callosum region visualized by MeDAS appeared to be much larger in the *Plp*-Akt-DD mouse brain than in the control littermate wild-type mouse brain, which was the same pattern that was observed in the Black-Gold or MBP antibody staining. Thus, MeDAS is a sensitive and specific probe for myelin.

2.4.2 Quantitative analysis—Following MeDAS staining, the hypermyelinated corpus callosum region in the *Plp*-Akt-DD mice brains appeared to be much larger than that in the control littermates' brains. The difference of MeDAS staining between *Plp*-Akt-DD and control littermates' brains was also analyzed by quantification of MeDAS fluorescent intensities on coronal tissue sections of both *Plp*-Akt-DD and control littermates. MeDAS fluorescent intensities on coronal tissue sections of both *Plp*-Akt-DD and control littermates were quantified in terms of pixel intensity value. Thus, images of MeDAS staining (from the midline to the cingulum, 8 per mouse) were acquired on a Leica DMR microscope (20 × objective). Quantification of fluorescent intensities was derived from the images depicted in Figure 3A, 3B. In the same ROI, the average fluorescent intensity in *Plp*-Akt-DD mice is much higher than that in control littermates. Quantitative analysis of the fluorescent intensity in the corpus callosum region shows that there was a significant increase in myelination in *Plp*-Akt-DD mice (126.6 ± 4.614) compared to control mice (97.88 ± 4.290) (*$p<0.05$, $n = 4$, Student's *t*-test). This is consistent with Black-Gold and MBP staining that has been previously reported.[15,19] Comparison of tissue staining between the hypermyelinated mouse model and control littermates indicated that MeDAS is a sensitive myelin probe that provides a means to detect myelin changes in the brain. Since fluorescent MeDAS readily passes across the blood-brain barrier, it can also be used to directly stain myelinated fibers *in situ* following administration through tail-vein injection.

2.4.3 *In Situ* Staining of Myelin—Following the *in vitro* studies, we explored the potential of MeDAS to stain myelin sheaths *in situ*. A dose of about 0.5 mg of MeDAS (25 mg/kg) was administered via tail vein injection to both *Plp*-Akt-DD and control littermates.

NIH-PA Author Manuscript

NIH-PA Author Manuscript

NIH-PA Author Manuscript

At 30 minutes post-injection, the mice were perfused with saline and 4% paraformaldehyde (PFA), and the brains were removed and sectioned as described above. Because MeDAS is inherently fluorescent, MeDAS staining of myelin was then directly examined by fluorescent microscopy. As shown in Figure 4A and 4B, MeDAS readily entered the brain and selectively labeled myelin sheaths in myelinated regions such as the corpus callosum. For comparison, Black-Gold staining in adjacent sections was also conducted (Figure 4C and 4D). The patterns of MeDAS staining were found to be consistent with that of Black-Gold staining, suggesting that MeDAS binds selectively to myelin fibers *in situ* in the white matter regions. In addition, MeDAS staining is sensitive to detecting the degree of myelination. In the corpus callosum of *Plp*-Akt-DD mice, MeDAS staining readily detects the enhancement of myelination, which had resulted in the enlargement of the corpus callosum region. These results indicate that MeDAS stains myelin *in situ* with high selectively and sensitivity.

2.5. Quantitative microPET imaging

Encouraged by the above *in vitro* and *ex vivo* studies, we then conducted *in vivo* microPET studies and quantitatively compared the level of myelination in *Plp*-Akt-DD *vs* the control littermates. In this study, we conducted both [^{11}C]MeDAS microPET imaging and high resolution MR imaging of the mouse brains. The *Plp*-Akt-DD and control littermates, were imaged side by side on the same bed for direct comparison. For quantitative analysis, the resultant microPET images were then registered to the MR images, which allowed us to accurately define the region of interest (ROI) and quantify the radioactivity concentrations. As shown in Figure 5, both whole brains and corpus callosums were used as ROI, and the radioactivity concentrations were determined in terms of standardized uptake values (SUV). Compared with the control mouse, the hypermyelination of *Plp*-Akt-DD mouse showed a significant increase of radioactivity concentration in both whole brains and corpus callosums during the 90 min PET scan. The average uptake in the corpus callosum in hypermyelinated mouse brain was 34% higher than that in the control littermate brain ($p < 0.01$).

These studies clearly demonstrated that [^{11}C]MeDAS-PET is a promising imaging marker for direct quantification of myelination *in vivo* in animal models. Following imaging studies, all of the animals survived and showed no sign of any behavioral changes, which indicates the radioligand has no apparent toxicity or any pharmacological effects.

2.6. *Ex vivo* autoradiography

As shown in Figure 5, the radioactivity concentration of [^{11}C]MeDAS in the corpus callosum region was significantly higher in *Plp*-Akt-DD mice than that in wild-type controls. Due to the relatively small size of the mouse brain, a partial volume effect may exist that should be excluded for a more rigorous comparison. To further evaluate *ex vivo* brain penetration, we conducted *ex vivo* autoradiography studies in the mouse brain by administering [^{11}C]MeDAS through tail vein injections. With relatively high resolution, *ex vivo* autoradiography permitted us to examine the distribution of [^{11}C]MeDAS in different brain regions. As shown in Figure 6A, distinct labeling of the corpus callosum, the area known to have a high density of myelinated sheaths, was observed after mouse brain tissue sections (coronal) were exposed to [^{11}C]MeDAS for 20 min, indicating that the autoradiographic visualization was consistent with histological staining of myelinated regions. Using MRI as a reference, autoradiographic visualization indicated that [^{11}C]MeDAS was retained selectively to those myelinated regions such as the corpus callosum (Figure 6B). To further demonstrate the binding specificity of [^{11}C]MeDAS to myelin sheaths, we performed *ex vivo* blocking study. Thus, mice were first injected i.v. with unlabelled BDB (5 mg/kg) that we have previously developed as a specific myelin-binding agent.[20,21] Five minutes later, [^{11}C]MeDAS was then administered also through tail

NIH-PA Author Manuscript

NIH-PA Author Manuscript

NIH-PA Author Manuscript

vein injection. After 10 min, the mice were sacrificed and the brain tissue were removed and sectioned. As shown in Figure 6C, pretreatment of the mice with unlabeled BDB significantly reduced the autoradiographic labeling of the corpus callosum. After 20 min exposure to [^{11}C]MeDAS, no distinct labeling of the corpus callosum was observed, indicating that [^{11}C]MeDAS binds to the myelinated corpus callosum with high specificity. This further confirms that the radioactivity signal detected by PET indeed reflects the specific spatial distribution of [^{11}C]MeDAS after binding to myelinated fibers, which is consistent with histological staining. Thus, the combination of *ex vivo* autoradiography with [^{11}C]MeDAS and with PET imaging studies confirmed that [^{11}C]MeDAS-PET is a specific imaging marker of myelination.

3. CONCLUSION

In this work, we demonstrated that a stilbene derivative, *N*-methyl-4,4′diamino stilbene ([^{11}C]MeDAS) binds to myelin fibers with high specificity and sensitivity. An *in vivo* biodistribution study in mice showed high permeability across the BBB. Distinct labeling of myelin fibers by [^{11}C]MeDAS was observed in the corpus callosum through *in situ* fluorescent staining and *ex vivo* autoradiography. Quantitative [^{11}C]MeDAS microPET studies permitted direct differentiation in myelination between *Plp*-Akt-DD mice and wild-type littermates. Taken together, these studies strongly suggest that [^{11}C]MeDAS is a promising myelin-imaging agent for PET studies that can serve to monitor myelin changes.

4. Experimental

4.1 General remarks

Black-Gold® (AG390) was purchased from Millipore, Bedford, MA. Anti-myelin basic protein (MBP) antibodies (*AB980*) were obtained from Chemicon-Millipore, Bedford, MA, and IRDye 800CW Goat Anti-Rabbit (926-32211) was purchased from *Li-COR Biosciences*, Lincoln, NE. SWR/J mice were obtained from the Jackson Laboratory, Bar Harbor, MN, and the *Plp*-Akt-DD mice were obtained as previously described.[15]

4.2 Radiosynthesis

Carbon-11 was produced in the form of [^{11}C]carbon dioxide ([^{11}C]CO_2) at Scanditronix MC17 cyclotron by nuclear reaction $^{14}N(p\alpha)^{11}C$. [^{11}C]CO_2 was trapped by a column prefilled with porapak Q at room temperature. The [^{11}C]CO_2 was then reacted with nanopowder nickel at high temperature (350 °C) to form methane, which was then trapped at −79 °C. Using direct iodination, [^{11}C] methane was converted to [^{11}C]CH_3I. [^{11}C]CH_3OTf was generated by reaction of the [^{11}C]CH_3I with silver triflate in an online flow at 200 °C using a helium gas at a flow rate of 50 mL/min. The [^{11}C]CH_3OTf was then bubbling into a reaction vial prefilled with 1-2 mg of DAS dissolved in 0.5 mL acetone at −30 °C Trapping was monitored with an isotope calibrator until the maximal value was attained. The radiomethylation reaction was then carried out at 90 °C for 2 min. After cooling to room temperature the reaction mixture was diluted with 1 mL of HPLC eluent and was subsequently transferred to the preparative radio-HPLC system. (Phenomenex C-18 column, 10μ, 250 mm × 10 mm, acetonitrile : H_2O = 60 : 40, flow rate 8.0 mL/min). The product containing fraction (retention time is about 5.1 min) was collected and was diluted with 25 mL of sterile water. The resulting mixture was subjected to solid-phase extraction using a C-18 Sep-Pak cartridge. The Sep-Pak was washed with another 10 mL of water and the final product was eluted with 1 mL of ethanol followed by 9 mL of sterile saline to formulate the product as isotonic solution. The decay-corrected radiochemical yield of [^{11}C]MeDAS obtained was in the range of 50 - 60%. The synthesis was completed in 50 - 60 min. Quality control of the product was carried out by an analytical radio-HPLC system (Phenomenex

NIH-PA Author Manuscript

NIH-PA Author Manuscript

NIH-PA Author Manuscript

C-18 column, 5μ, 250 mm × 4.6 mm, acetonitrile: H_2O = 60 : 40, flow rate 1.0 mL/min). Identification of the product and chemical radiochemical purities were verified by co-injection with the non-labeled standard of MeDAS which has the same retention time (6.77 min) on the UV and the radioactive chromatograms. Quality control by radio-HPLC showed a radiochemical purity of > 95% with specific activities up to 80 ± 30 GBq/μmol (EOS).

4.3 Measurement of Partition Coefficients (logPoct)

Partition coefficient values were measured by mixing [^{11}C]MeDAS (radiochemical purity is greater than 98%, approximately 500,000 cpm) with *n*-octanol (3 g, 3.65 mL) and sodium phosphate buffer (PBS, 0.1 mol/mL, 3 g, 3.0 mL, pH 7.40) in a test tube. The test tube was vortexed for 3 min at room temperature, followed by centrifugation at 3500 rpm for 5 min. Then an aliquot of 1 mL buffer and 1 mL *n*-octanol were removed, weighed, and counted. Samples from the remaining *n*-octanol layer were removed and re-partitioned until consistent partitions of coefficient values were obtained. The partition coefficient value was determined by calculating the ratio of cpm/g of *n*-octanol to that of PBS and expressed as logPoct = log[cpm/g (*n*-octanol)/cpm/g(PBS)]. All assays were performed in triplicate.

4.4 *In vitro* tissue staining of corpus callosum in *Plp*-Akt-DD and wild type mice

Plp-Akt-DD and wild type mice were deeply anesthetized and perfused transcardially with saline (10 mL) followed by fixation with 4% PFA in PBS (10 mL, 4 °C, pH 7.6). Brain tissues were then removed, postfixed by immersion in 4% PFA overnight, dehydrated in 30% sucrose solution, embedded in freezing compound (OCT, Fisher Scientific, Suwanee, GA), cryostat sectioned at 10 μm on a microtome and mounted on superfrost slides (Fisher Scientific). Both brain sections were incubated with MeDAS [10 μM, 1% DMSO in 1 × PBS (pH 7.0)] for 20 minutes at room temperature in the dark. Excess compound was washed by briefly rinsing the slides in PBS (1×) and coverslipped with fluoromount-G mounting media (Vector Laboratories, Burlingame, CA). Sections were then examined under a Leica DRMB microscope equipped for fluorescence.

For comparison, immunohistochemistry of MBP staining was performed in both adjacent sections. Brain sections (*Plp*-Akt-DD and wild type) mounted on slides were incubated in a solution containing anti-MBP mAb primary antibody (rabbit anti-MBP 1:2000, Chemicon-Millipore, Bedford, MA) diluted in 3% normal goat serum and stored overnight at 4 °C. Following 3 rinses with PBS, sections were then incubated in IRDye 800CW Goat Anti-Rabbit (LI-COP biosciences, Lincoln, NE) (diluted 1:5000 in PBS with 3% normal donkey serum) for 1 hour at 37 °C, then washed 3 times with PBS. Images were obtained on a LI-COR *Odyssey* infrared imaging system (LI-COR Biosciences, Lincoln, NE).

4.5 *Ex Vivo* tissue staining of corpus callosum in *Plp*-Akt-DD and wild type mice

Under anesthesia, *Plp*-Akt-DD and wild type mice were injected with MeDAS (25 mg/kg) via the tail vein, and 30 min later the mice were then perfused transcardially with saline (10 mL) followed by 4% PFA in PBS (10 mL, 4°C, pH 7.6). Brain tissues were then separately removed, postfixed by immersion in 4% PFA overnight, dehydrated in 30% sucrose solution, cryostat sectioned at 10 μm on a microtome, and mounted on superfrost slides (Fisher Scientific), and imaged directly under fluorescent microscopy as described above.

For comparison, Black-Gold staining was performed on the same sections. The sections were washed with saline, incubated for 20 minutes with 0.3% Black-Gold solution at 60 °C, washed twice with saline, fixed for 3 minutes in 2% sodium thiosulfate, and mounted using fluoromount-G mounting media (Vector Laboratories; Burlingame, CA).

NIH-PA Author Manuscript

NIH-PA Author Manuscript

NIH-PA Author Manuscript

4.6 Quantification and statistical analysis

Images of MeDAS staining (from the midline to the cingulum, 8 per mouse) were acquired on a Leica DMR microscope (20 × objective) with an Optronics Magnafire digital camera. *ImageJ* software (http://rsb.info.nih.gov/ij/) was used to quantify pixel intensity values. The corpus callosum between the midline and below the apex of the cingulum was selected as the region of interest (ROI). The images were normalized by setting the threshold to exclude values that are below Black-Gold reactivity. The fluorescent intensity in the ROI of WT mice was given an arbitrary value of 100, and the fluorescent intensity in the same ROI of *Plp*-Akt-DD mice was determined as a percentage of that in the WT mice. The data were analyzed using a GraphPad Prism (*GraphPad Software*, La Jolla, CA) with a nonpaired Student's *t* test.

4.7 Brain uptake studies in mice

[^{11}C]MeDAS was administered to Swiss-Webster mice weighing 20-25 g following i.v. tail-vein injection of up to 3.7 MBq (100 μCi). The brains of 3 animals were removed at 5, 30 and 60 min post-injection, weighed and counted for radioactivity. The brain uptake values of the decay corrected activity were expressed as a percentage of injected doses per organ.

4.8 Biodistribution studies in mice

In order to provide an estimate of human dosimetry, whole body distribution studies were conducted in mice. Thus, ca. 3.7 MBq (100 μCi) of [^{11}C]MeDAS was administered to mice through tail vein injection and the animals were weighed and euthanized at 5, 30, and 60 min via cardiac excision. Organs of interest (heart, liver, spleen, lung, kidney, stomach, and intestine) were removed, and radioactivity concentration (%ID/organ) of each organ was determined using an automatic gamma well-counter.

4.9 *Ex vivo* autoradiography in mice brain

Two wild-type mice were sacrificed by CO_2 euthanasia at 10 min post i.v. injection of [^{11}C]MeDAS (111 MBq, 3.0 mCi). For blocking studies, another two wild-type mice were pretreated with BDB (5 mg/kg) 5 min prior of the injection of [^{11}C]MeDAS (111 MBq, 3.0 mCi) into the tail vein. Mice were sacrificed by CO_2 euthanasia at 10 min post i.v. injection of [^{11}C]MeDAS (111 MBq, 3.0 mCi). The brains were rapidly removed, placed in O.C.T. embedding medium and frozen at −20 °C. After reaching equilibrium at this temperature, the brains were coronally cryostat sectioned at 20 μm and mounted on superfrost slides (Fisher Scientific). After drying by air at room temperature, the slides were put in a cassette and exposed to film for 20 min to obtain images.

4.10 Magnetic Resonance Imaging (MRI) studies

All MR imaging experiments were performed on a Bruker Biospec 7.0T/30 cm MRI and Spectroscopy scanner (Bruker Biospin, Billerica, MA). The animal's head was positioned in a 72-mm volume ID cylindrical transceiver coil. A RARE acquisition (TR/TE=2000/40ms, 4 echoes, FOV = 45 mm × 45 mm, matrix = 256 × 256) was used to acquire 15 contiguous 1-mm axial images of each animal's brain.

4.11 MicroPET studies

Animals were placed in a Concord R4 microPET scanner (Knoxville, TN) under anesthesia. After a 10 min transmission scan with a Co-57 source, 7.4 MBq of [^{11}C]MeDAS were administered to each animal through a tail vein injection, which was immediately followed by dynamic acquisition for up to 90 min. A 2-D filtered back projection (FBP) algorithm was used for image reconstruction with a 256 × 256 pixel resolution per transverse slice. A total of 63 transverse slices were reconstructed with the field of view covering the head of

NIH-PA Author Manuscript

NIH-PA Author Manuscript

NIH-PA Author Manuscript

the animals. Decay correction, attenuation correction, and scatter correction were all performed during the image histogram and reconstruction processes.

4.12 Co-registration of Images and Statistical Analysis

Coregistration of MRI and PET images were conducted by using the MATLAB-based program COMKAT (Compartmental Model Kinetic Analysis Tool). The registration was conducted using a coronal view of the mice. After creating uniform images from the PET and MRI images, VOI (Volume of interest) and ROI (Region of interest) were defined and used to measure the radioactivity concentration in the corpus callosums of both hypermyelinated and wild type mice. Multiple time activity curves were then obtained for statistical analysis.

The radioactivity was decay-corrected and normalized by the body weight of the mice and the amount of [^{11}C]MeDAS injected. The resulting normalized time-activity curves obtained from different data sets were averaged to provide normalized time-activity curves for the experiments. A student t-test was used to evaluate if there was any significant difference between the curves with a p value < 0.05.

Supplementary Material

Refer to Web version on PubMed Central for supplementary material.

Acknowledgments

We gratefully acknowledge financial support through grants from the Department of Defense, National Multiple Sclerosis Society, and NIH/NINDS (R01 NS061837). We also thank George Bakale for assistance in preparation of the manuscript.

References and notes

1. Hildebrand C, Remahl S, Persson H, Bjartmar C. Prog Neurobiol 1993;40:319. [PubMed: 8441812]
2. Compston A, Coles A. Lancet 2002;359:1221. [PubMed: 11955556]
3. Hauw JJ, Delaere P, Seilhean D, Cornu P. J Neuroimmunol 1992;40:139. [PubMed: 1430147]
4. Colburn WA. J Clin Pharmacol 2003;43:329. [PubMed: 12723454]
5. Ozturk A, Smith S, Gordon-Lipkin E, Harrison D, Shiee N, Pham D, Caffo B, Calabresi P, Reich D. Mult Scler 16:166. [PubMed: 20142309]
6. Leist TP, Marks S. Neurology 74(Suppl 1):S54. [PubMed: 20038764]
7. Filippi M, Rocca MA, Comi G. Lancet Neurol 2003;2:337. [PubMed: 12849150]
8. Rovaris M, Filippi M. Curr Opin Neurol 1999;12:337. [PubMed: 10499178]
9. Molyneux PD, Barker GJ, Barkhof F, Beckmann K, Dahlke F, Filippi M, Ghazi M, Hahn D, MacManus D, Polman C, Pozzilli C, Kappos L, Thompson AJ, Wagner K, Yousry T, Miller DH. Neurology 2001;57:2191. [PubMed: 11756596]
10. Phelps ME. Proc Natl Acad Sci U S A 2000;97:9226. [PubMed: 10922074]
11. Chen MK, Guilarte TR. Toxicol Sci 2006;91:532. [PubMed: 16554315]
12. Wilms H, Claasen J, Rohl C, Sievers J, Deuschl G, Lucius R. Neurobiol Dis 2003;14:417. [PubMed: 14678758]
13. Cuzner ML. Biochem Soc Trans 1997;25:671. [PubMed: 9191179]
14. Wu C, Wei J, Tian D, Feng Y, Miller RH, Wang Y. J Med Chem 2008;51:6682. [PubMed: 18844339]
15. Flores AI, Narayanan SP, Morse EN, Shick HE, Yin X, Kidd G, Avila RL, Kirschner DA, Macklin WB. J Neurosci 2008;28:7174. [PubMed: 18614687]
16. Levin VA. J Med Chem 1980;23:682. [PubMed: 7392035]

NIH-PA Author Manuscript

NIH-PA Author Manuscript

NIH-PA Author Manuscript

17. Dishino DD, Welch MJ, Kilbourn MR, Raichle ME. J Nucl Med 1983;24:1030. [PubMed: 6605416]
18. Hashimoto K, Inoue O, Suzuki K, Yamasaki T, Kojima M. Ann Nucl Med 1989;3:63. [PubMed: 2561896]
19. Narayanan SP, Flores AI, Wang F, Macklin WB. J Neurosci 2009;29:6860. [PubMed: 19474313]
20. Wu C, Tian D, Feng Y, Polak P, Wei J, Sharp A, Stankoff B, Lubetzki C, Zalc B, Mufson EJ, Gould RM, Feinstein DL, Wang Y. J Histochem Cytochem 2006;54:997. [PubMed: 16709728]
21. Wang Y, Wu C, Caprariello AV, Somoza E, Zhu W, Wang C, Miller RH. J Neurosci 2009;29:14663. [PubMed: 19923299]

NIH-PA Author Manuscript

NIH-PA Author Manuscript

NIH-PA Author Manuscript

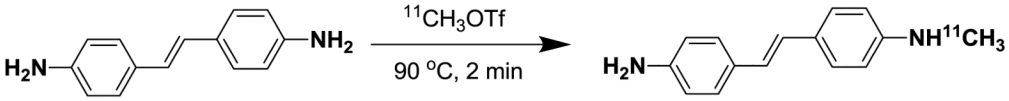

Scheme 1.

Radiosynthesis of [^{11}C]MeDAS through radiomethylation of (*E*)-4,4′-diaminostilbene with [^{11}C]methyl triflate

NIH-PA Author Manuscript

NIH-PA Author Manuscript

NIH-PA Author Manuscript

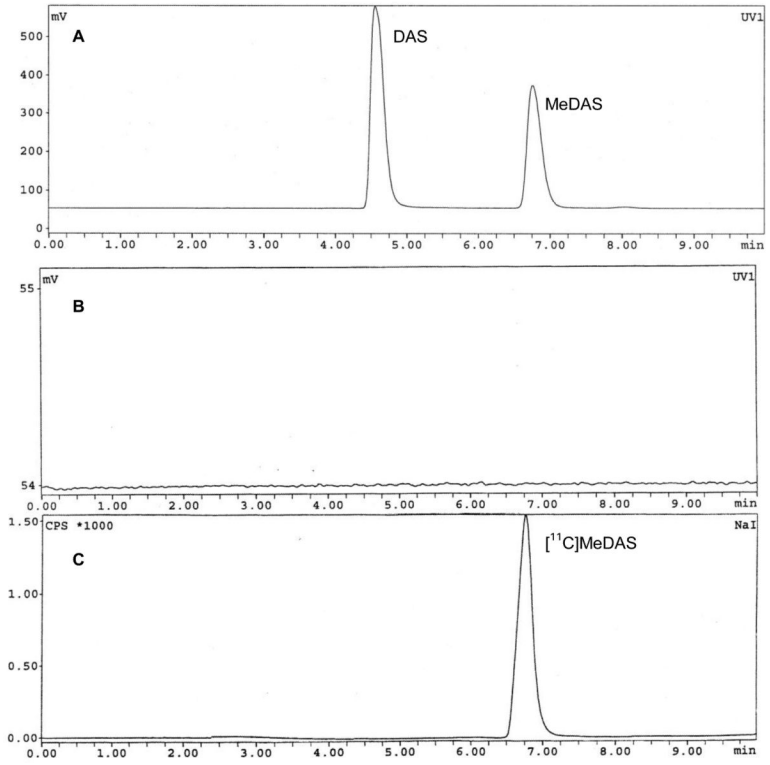

Figure 1.

Quality control HPLC figures for both UV and radioactive peaks. **A**: Coinjection of precursor DAS and non-labeled cold standard of MeDAS, the rentention times were 4.57 min and 6.77 min, respectively. **B**: Quality control by analytical radio-HPLC showed the quantity of the precursor DAS in the final product is negligible: no DAS residue was detected after HPLC purification. **C**: Quality control by analytical radio-HPLC showed a radiochemical purity of the final product is greater than 95%, the retention time of [^{11}C[MeDAS was 6.77 min, which was consistent with the non labeled cold standard MeDAS.

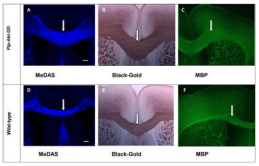

Figure 2.

In vitro MeDAS staining (**A** and **D**) of myelin sheaths in corpus callosum in comparison with Black-Gold (**B** and **E**) and MBP staining (**C** and **F**) in adjacent sections. Arrows show myelinated corpus callosum. **A-C**, *Plp*-Akt-DD mouse brain sections stained with MeDAS, Black-Gold and MBP, respectively. **D-F**, Control mouse brain sections stained with MeDAS, Black-Gold and MBP, respectively. The corpus callosum region visualized by MeDAS appeared to be much larger in the *Plp*-Akt-DD mouse brain than in the control littermate wild-type mouse brain, which was the same pattern that was observed in the Black-Gold or MBP antibody staining.

NIH-PA Author Manuscript
NIH-PA Author Manuscript
NIH-PA Author Manuscript

NIH-PA Author Manuscript

NIH-PA Author Manuscript

NIH-PA Author Manuscript

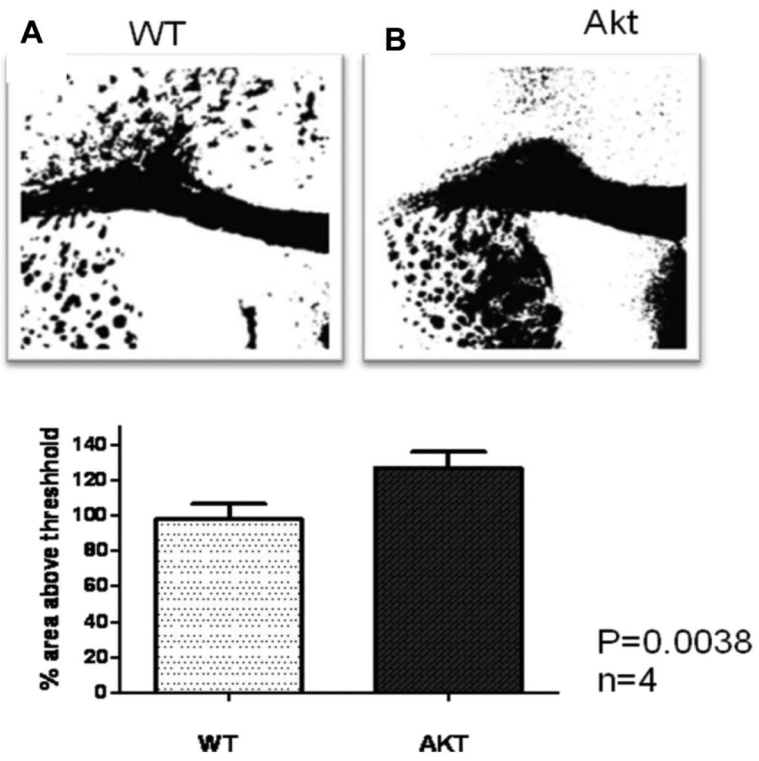

Figure 3.

Enhanced fluorescent density of MeDAS in the corpus callosum of *Plp*-Akt-DD mice. (**A**) Coronal brain sections of WT (SWR/J) and *Plp*-Akt-DD mice at 5 months age were stained with MeDAS, showing an enlarged corpus callosum in the *Plp*-Akt-DD mice. (**B**) Quantification of fluorescent density estimated from MeDAS staining of WT and *Plp*-Akt-DD corpus callosum. The area of the corpus callosum between the midline and below the apex of the cingulum was quantified. Quantitative analysis revealed a significant increase in myelin density in the corpus callosum of *Plp*-Akt-DD mice as compared to WT (*$p<0.05$, $n = 4$, Student's *t*-test).

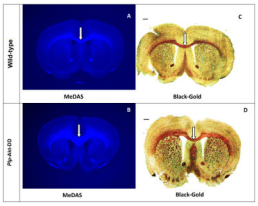

Figure 4.

In situ MeDAS staining of myelin sheaths in the corpus callosum in correlation with Black-Gold staining. (**A, B**) In situ staining of MeDAS in the control (**A**) vs hypermyelinated mouse brains (**B**). (**C, D**) Black-Gold staining in the control (**C**) and hypermyelinated mouse brains (**D**) in adjacent sections, respectively. In the corpus callosum of *Plp*-Akt-DD mice, MeDAS staining readily detects the enhancement of myelination, which had resulted in the enlargement of the corpus callosum region. Arrows show myelinated corpus callosum.

NIH-PA Author Manuscript
NIH-PA Author Manuscript
NIH-PA Author Manuscript

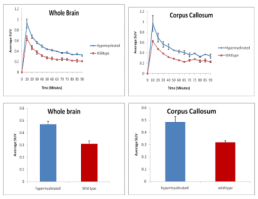

Figure 5.

Average radioactivity concentration of [^{11}C]MeDAS in the whole brain and corpus callosum in terms of standardized uptake value (SUV) as a function of time in control (red) and hypermyelinated (blue) mice.

NIH-PA Author Manuscript
NIH-PA Author Manuscript
NIH-PA Author Manuscript

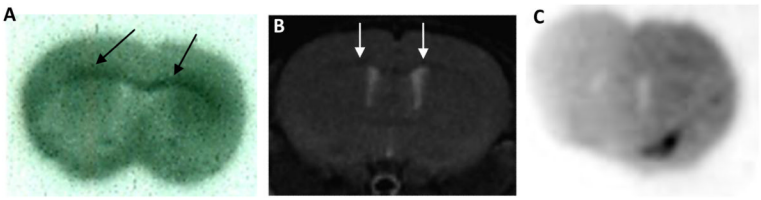

Figure 6.

Ex vivo film autoradiography. (**A**) [^{11}C]MeDAS binding to myelinated corpus callosum in mouse brain (coronal). Arrows show myelinated corpus callosum labeled by [^{11}C]MeDAS. (**B)** The autoradiographic visualization was further confirmed by using MRI as reference, indicating that the autoradiographic visualization was consistent with histological staining of myelinated region. (**C**) No distinct labeling of the corpus callosum was observed after pretreatment of the mice with unlabeled BDB (5 mg/kg), indicating that [^{11}C]MeDAS binds to myelinated corpus callosum with high selectivity and specificity.

NIH-PA Author Manuscript NIH-PA Author Manuscript NIH-PA Author Manuscript

NIH-PA Author Manuscript

NIH-PA Author Manuscript

NIH-PA Author Manuscript

Table 1

Biodistribution of [^{11}C] MeDAS in Swiss-Webster mice (%ID/organ ± SD, n=3)

Organ	5 min	30 min	60 min
Heart	0.40 ± 0.02	0.33 ± 0.09	0.75 ± 0.22
Liver	15.86 ± 0.74	10.83 ± 1.11	7.75 ± 0.25
Spleen	0.28 ± 0.01	0.39 ± 0.14	0.90 ± 0.46
lung	0.85 ± 0.06	0.76 ± 0.26	1.20 ± 0.29
Kidney	2.69 ± 0.13	2.00 ± 0.23	1.78 ± 0.33
Stomach	1.00 ± 0.12	0.67 ± 0.30	1.21 ± 0.33
intestine*	0.42 ± 0.12	0.65 ± 1.06	1.74 ± 0.45
Brain	2.56 ± 0.04	1.05 ± 0.05	1.37 ± 0.51

*: %ID/gram